Report

Neuron

The Forebrain Thirst Circuit Drives Drinking through Negative Reinforcement

Highlights

- The genes *Agtr1a* and *Adcyap1* label thirst neurons in the OVLT and MnPO, respectively
- SFO, OVLT, and MnPO thirst neurons control both drinking and blood pressure
- Stimulation of thirst neurons in SFO, OVLT, and MnPO is negatively reinforcing
- MnPO projections dissociate the cardiovascular and behavioral outputs of the LT

Authors

David E. Leib, Christopher A. Zimmerman, Ailar Poormoghaddam, ..., Chan Lek Tan, Yiming Chen, Zachary A. Knight

Correspondence

zachary.knight@ucsf.edu

In Brief

Leib et al. reveal the motivational mechanism by which the thirst circuit drives drinking. They show that molecularly defined cell types in three forebrain nuclei promote drinking by drive reduction and also coordinate the cardiovascular response to fluid imbalance.

Leib et al., 2017, Neuron *96*, 1272–1281
December 20, 2017
https://doi.org/10.1016/j.neuron.2017.11.041

CellPress

CellPress

Neuron
Report

The Forebrain Thirst Circuit Drives Drinking through Negative Reinforcement

David E. Leib,[1,2,3,4] Christopher A. Zimmerman,[1,2,3,4] Ailar Poormoghaddam,[1,2] Erica L. Huey,[1,2] Jamie S. Ahn,[1,2] Yen-Chu Lin,[1,2] Chan Lek Tan,[1,2] Yiming Chen,[1,2,3] and Zachary A. Knight[1,2,3,5,*]
[1]Department of Physiology
[2]Kavli Institute for Fundamental Neuroscience
[3]Neuroscience Graduate Program
University of California, San Francisco, San Francisco, CA 94158, USA
[4]These authors contributed equally
[5]Lead Contact
*Correspondence: zachary.knight@ucsf.edu
https://doi.org/10.1016/j.neuron.2017.11.041

SUMMARY

The brain transforms the need for water into the desire to drink, but how this transformation is performed remains unknown. Here we describe the motivational mechanism by which the forebrain thirst circuit drives drinking. We show that thirst-promoting subfornical organ neurons are negatively reinforcing and that this negative-valence signal is transmitted along projections to the organum vasculosum of the lamina terminalis (OVLT) and median preoptic nucleus (MnPO). We then identify molecularly defined cell types within the OVLT and MnPO that are activated by fluid imbalance and show that stimulation of these neurons is sufficient to drive drinking, cardiovascular responses, and negative reinforcement. Finally, we demonstrate that the thirst signal exits these regions through at least three parallel pathways and show that these projections dissociate the cardiovascular and behavioral responses to fluid imbalance. These findings reveal a distributed thirst circuit that motivates drinking by the common mechanism of drive reduction.

INTRODUCTION

Eating and drinking are fundamental motivated behaviors, but how the brain transforms the need for food or water into a specific motivational drive remains poorly understood. Traditionally, two broad classes of mechanisms have been proposed to motivate behavior (Berridge, 2004). The first involves the ability of food or water deprivation to magnify the rewarding properties of eating or drinking and thereby positively reinforce these behaviors. This is the mechanism that makes food taste more delicious when you are hungry, a phenomenon known as alliesthesia (Cabanac, 1971; Toates, 1986). On the other hand, food and water deprivation are experienced as intrinsically unpleasant states, and therefore, animals will perform work simply to avoid these aversive conditions, a mechanism known as negative reinforcement or drive reduction (Hull, 1943; Spence, 1956). Under normal conditions, these two processes are thought to work together to motivate behavior, but it remains unknown how they are each instantiated in the brain at the level of specific neural circuits.

For the control of drinking behavior, the critical neurons that sense and respond to changes in internal state are located within three small, interconnected forebrain nuclei known collectively as the lamina terminalis (LT). These structures include the subfornical organ (SFO) and organum vasculosum of the lamina terminalis (OVLT), which are situated outside the blood-brain barrier and contain interoceptive neurons that monitor the blood directly (McKinley et al., 2003), and the median preoptic nucleus (MnPO), which is thought to function as a downstream integratory site (McKinley et al., 2015). When the blood volume falls or osmolarity rises, neurons within these three nuclei become activated, thereby triggering thirst, salt appetite, and an array of autonomic and neuroendocrine outputs that function to restore fluid balance (Bourque, 2008; McKinley and Johnson, 2004; Noda and Sakuta, 2013; Zimmerman et al., 2017).

Given its preeminent role in the control of drinking behavior, the LT represents a logical starting point for investigation of the motivational processes underlying thirst. However, this investigation has been complicated by the fact that each structure within the LT is neurochemically heterogeneous, and the specific cell types that control drinking in the OVLT and MnPO have not been fully characterized (Abbott et al., 2016; Zimmerman et al., 2017). In the SFO, a population of glutamatergic neurons defined by expression of the genes *Nos1*, *Etv1*, and *Camk2* (SFO^{GLUT} neurons) are activated during thirst and are necessary and sufficient for drinking behavior (Betley et al., 2015; Matsuda et al., 2017; Nation et al., 2016; Oka et al., 2015; Zimmerman et al., 2016). Furthermore, stimulation of SFO^{GLUT} neurons has negative valence (Betley et al., 2015). However, it remains unclear whether this negative-valence signal is the mechanism by which SFO^{GLUT} neurons motivate behavior, because it has not been demonstrated that animals will perform work to shut off this signal, which is the hallmark of negative-reinforcement learning (Teitelbaum, 1966).

To address these questions, we have systematically investigated the cells, pathways, and motivational mechanisms by which the forebrain thirst circuit generates drinking behavior.

RESULTS

SFO^{GLUT} Neurons Coordinate the Behavioral and Autonomic Responses to Fluid Imbalance

We first targeted channelrhodopsin-2 (ChR2) to SFO^{GLUT} neurons and implanted an optical fiber above the SFO (Figure 1A). As previously reported, photostimulation of SFO^{GLUT} neurons triggered voracious and specific water consumption (Figures 1B and 1C) (Betley et al., 2015; Oka et al., 2015; Zimmerman et al., 2016). Photostimulation of SFO^{GLUT} neurons also triggered a rapid and reversible increase in blood pressure (Figure 1D; Figure S1), which likely functions to increase blood circulation in response to acute drops in blood volume (Mangiapane and Simpson, 1980). These results indicate that glutamatergic neurons in the SFO coordinate both the behavioral and the autonomic responses to fluid imbalance.

Stimulation of SFO^{GLUT} Neurons and Their Projections Is Negatively Reinforcing

We next trained mice with daily sessions in which they were exposed to tonic photostimulation while given access to two levers, one of which induced a pause in photostimulation and the other of which was inactive (Figure 1E). After training in this negative-reinforcement paradigm, mice expressing ChR2 in SFO^{GLUT} neurons preferentially pressed the active lever to pause photostimulation (Figure 1E). In contrast, control mice expressing GFP in SFO^{GLUT} neurons showed no response to photostimulation in any assay. These data demonstrate that mice will perform instrumental responses to reduce SFO^{GLUT} neuron activity and therefore that the activity of these neurons is negatively reinforcing.

The SFO drives thirst via projections to two other LT structures, the OVLT and MnPO (Matsuda et al., 2017; Zimmerman et al., 2016). To test whether SFO^{GLUT} neurons transmit a negative-reinforcement signal to these downstream sites, we targeted ChR2 to SFO^{GLUT} neurons and implanted an optical fiber above the MnPO (Figure 1F). This fiber placement results in stimulation of axons innervating the MnPO as well as fibers of passage targeting the OVLT. We first confirmed that photostimulation of SFO^{GLUT}→MnPO/OVLT axons drives robust and specific water consumption (Figures 1G and 1H) and elevates blood pressure (Figure 1I) to an extent comparable to stimulation of SFO^{GLUT} neuron somas. We then trained these mice in the negative-reinforcement paradigm described above, which revealed that mice will robustly lever press to prevent photostimulation of SFO^{GLUT}→MnPO/OVLT projections (Figure 1J). Thus, projections from SFO^{GLUT} neurons to the OVLT and/or MnPO relay a negative-reinforcement signal that corresponds with the ability of these projections to drive drinking.

OVLT^{Agtr1a} Neurons Are Activated by Hyperosmolarity, and Their Activation Drives Drinking and Hypertension

The OVLT and MnPO were first implicated in the control of drinking behavior decades ago (Buggy and Jonhson, 1977), but the molecular identity of thirst-promoting neurons in these structures has remained unclear (Zimmerman et al., 2017). We first focused on the OVLT, which, like the SFO, lies outside the blood-brain barrier and therefore has unfettered access to circulating signals that stimulate thirst. The angiotensin 1A receptor (encoded by the *Agtr1a* gene) is expressed in the OVLT (Gonzalez et al., 2012; Lenkei et al., 1997) and is involved in the control of drinking behavior (Crews and Rowland, 2005). We used an Agtr1a-GFP reporter line (Gonzalez et al., 2012) to examine whether OVLT^{Agtr1a} neurons are activated by salt challenge (350 μL intraperitoneal injection of 2 M NaCl), a stimulus that rapidly increases plasma osmolarity and robustly triggers thirst (Figure 2A). This revealed extensive (70% ± 3% Fos^{+} neurons were GFP^{+}) and specific (64% ± 7% GFP^{+} neurons were Fos^{+}) co-localization between Fos induced by salt challenge and Agtr1a-GFP, suggesting that the *Agtr1a* gene may label thirst-promoting neurons in the OVLT. To gain genetic access to these cells, we generated a knockin mouse line that expresses Cre recombinase in frame with the endogenous *Agtr1a* gene (Agtr1a-2A-Cre mice; Figure 2B; Figure S2). Crossing this knockin line to a Cre-dependent GFP reporter line revealed recombination that was remarkably specifically localized to the OVLT relative to adjacent structures (Figure 2C; Figure S2). Neurochemical characterization by *in situ* hybridization revealed that OVLT^{Agtr1a} neurons primarily express Vglut2 (*Slc17a6*), but not Vgat (*Slc32a1*), indicating that these cells are predominantly glutamatergic (Figure 2J; see Figure S2 for additional discussion). Thus, the Agtr1a-2A-Cre mouse line provides genetic access to a specific population of OVLT neurons that are activated during thirst.

We next targeted ChR2 to OVLT^{Agtr1a} neurons and positioned an optical fiber above the OVLT. Photostimulation of these cells induced robust water intake that was time-locked to the onset of stimulation (Figure 2D), specific to water relative to hypertonic NaCl (Figures 2E and 2F) and food (Figure S2), and absent from control mice. Photostimulation also caused a rapid and reversible increase in blood pressure (Figure 2G; Figure S2). These data indicate that OVLT^{Agtr1a} neurons are sufficient to trigger the homeostatic responses to fluid imbalance.

Stimulation of OVLT^{Agtr1a} Neurons Is Negatively Reinforcing

We next investigated the motivational mechanisms by which OVLT^{Agtr1a} neurons drive drinking behavior. We first trained mice to perform a fixed ratio 3 (FR3) task, in which delivery of each drop of water requires three presses of an active lever (Figure 2H). Photostimulation of OVLT^{Agtr1a} neurons caused otherwise water-sated mice to vigorously and preferentially press the active lever to receive water (Figure 2H). Thus, stimulation of OVLT^{Agtr1a} neurons drives instrumental responding for water, indicating that these cells promote drinking through a specific change in motivational state rather than through a general enhancement of activity or ingestive behavior. We then trained mice in the negative-reinforcement paradigm described above, which revealed that mice will selectively lever press to prevent photostimulation of OVLT^{Agtr1a} neurons (Figure 2I). Thus, OVLT^{Agtr1a} neurons, like SFO^{GLUT} neurons, are activated by deviations from fluid homeostasis, are sufficient to generate robust thirst and cardiovascular responses, and motivate instrumental responding via negative reinforcement.

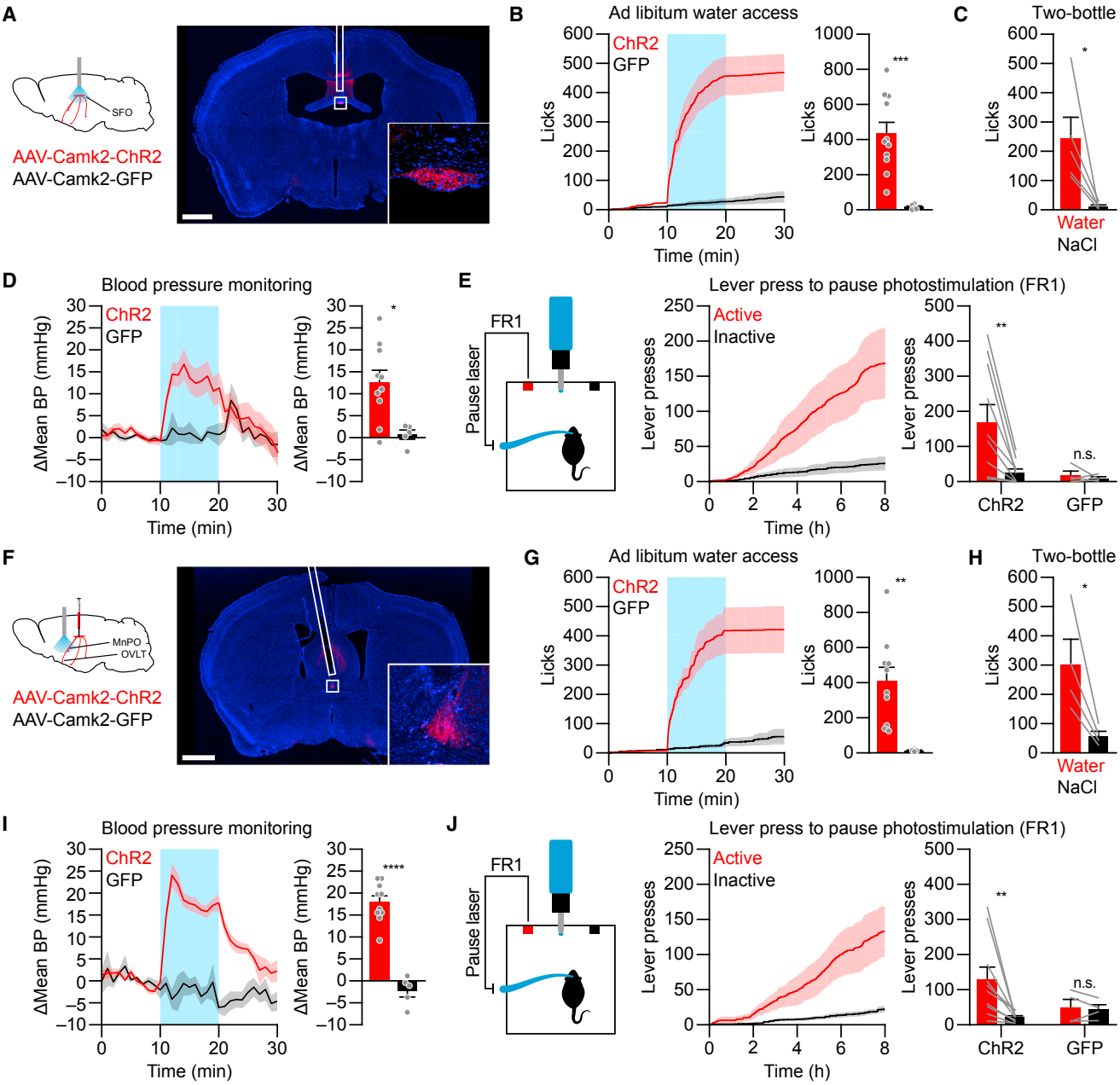

Figure 1. SFO Thirst Neurons Are Negatively Reinforcing

(A) Schematic of SFO^{GLUT} neuron photostimulation (left). ChR2-mCherry expression and optical fiber placement (right; scale bar, 1 mm).

(B) Cumulative drinking (left) and total drinking during photostimulation (right) by ChR2 (n = 11) and GFP (n = 5) mice.

(C) Total drinking during photostimulation by ChR2 mice (n = 5) with access to water and 0.3 M NaCl.

(D) Change in mean arterial blood pressure over time (left) and average photostimulation-induced change (right) for ChR2 (n = 10) and GFP (n = 5) mice.

(E) Schematic of negative-reinforcement experiment (left). Cumulative lever presses by ChR2 mice (middle). Total lever presses by ChR2 (n = 10) and GFP (n = 4) mice (right).

(F) Schematic of SFO^{GLUT}→MnPO/OVLT axon photostimulation (left). ChR2-mCherry expression and optical fiber placement (right; scale bar, 1 mm).

(G) Cumulative drinking (left) and total drinking during photostimulation (right) by ChR2 (n = 10) and GFP (n = 5) mice.

(H) Total drinking during photostimulation by ChR2 mice (n = 4) with access to water and 0.3 M NaCl.

(I) Change in mean arterial blood pressure over time (left) and average photostimulation-induced change (right) for ChR2 (n = 10) and GFP (n = 5) mice.

(J) Schematic of negative-reinforcement experiment (left). Cumulative lever presses by ChR2 mice (middle). Total lever presses by ChR2 (n = 10) and GFP (n = 4) mice (right).

Values are reported as mean ± SEM. *p < 0.05; **p < 0.01; ***p < 0.001; ****p < 0.0001. See also Figure S1.

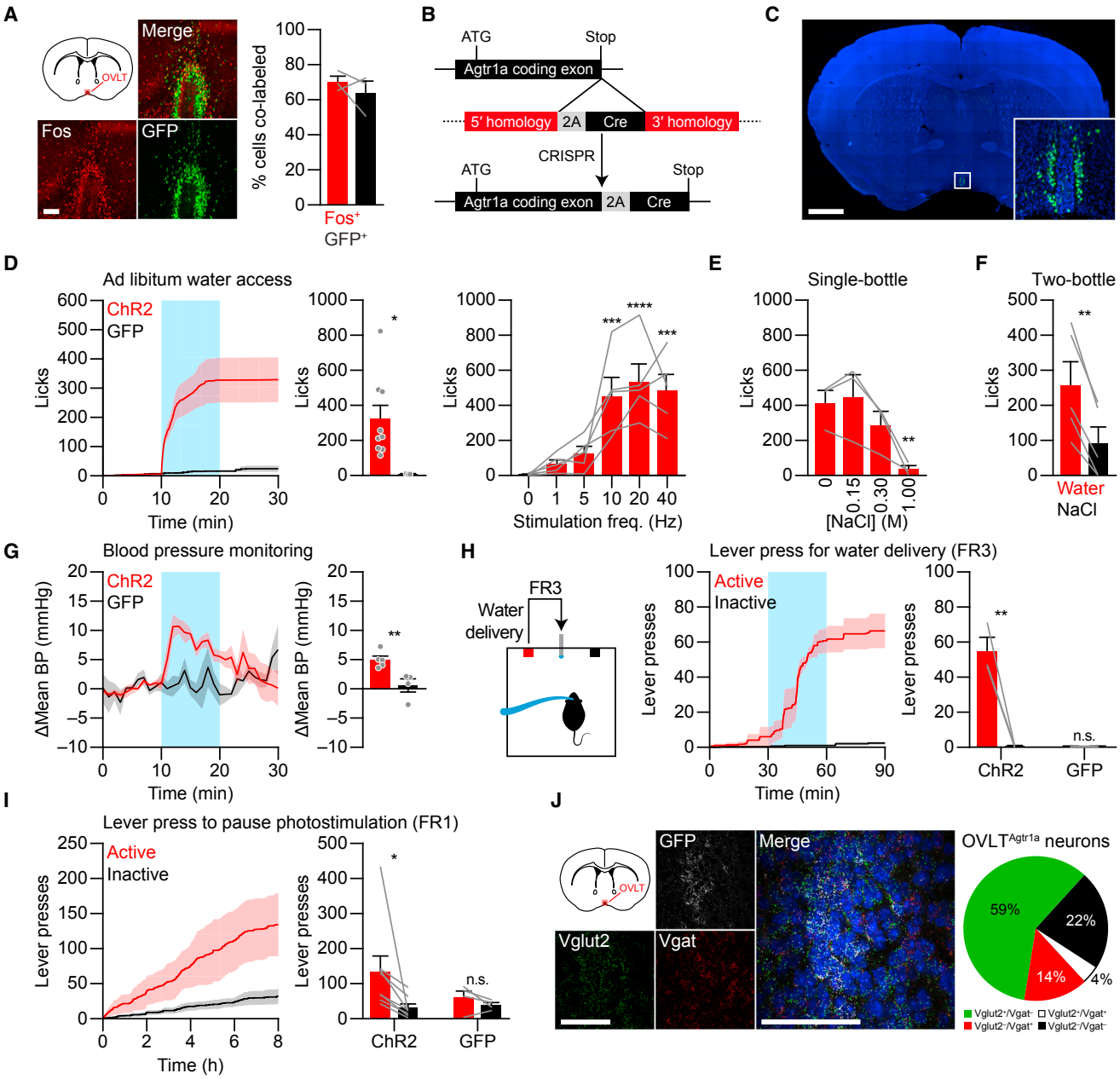

Figure 2. OVLT^{Agtr1a} Neurons Drive Thirst and Hypertension and Are Negatively Reinforcing

(A) Colocalization of Agtr1a-GFP and Fos induced by salt challenge in the OVLT of BAC transgenic mice (left; scale bar, 100 μm). Quantification (right; n = 3).

(B) Schematic for generation of Agtr1a-2A-Cre knockin mouse line by CRISPR-mediated homologous recombination.

(C) Histology showing GFP expression in the OVLT of Agtr1a-2A-Cre mice crossed to a GFP reporter line (scale bar, 1 mm).

(D) Cumulative drinking (left) and total drinking during photostimulation (middle) by ChR2 (n = 8) and GFP (n = 4) mice. Total drinking during photostimulation by ChR2 mice (n = 5) at different photostimulation frequencies (right).

(E) Total drinking during photostimulation by ChR2 mice (n = 3) with access to various NaCl solutions.

(F) Total drinking during photostimulation by ChR2 mice (n = 5) with access to water and 0.3 M NaCl.

(G) Change in mean arterial blood pressure over time (left) and average photostimulation-induced change (right) for ChR2 (n = 5) and GFP (n = 4) mice.

(H) Schematic of instrumental responding for water access experiment (left). Cumulative lever presses by ChR2 mice (middle). Total lever presses during photostimulation by ChR2 (n = 3) and GFP (n = 3) mice (right).

(I) Cumulative lever presses by ChR2 mice in the negative-reinforcement experiment (left). Total lever presses by ChR2 (n = 8) and GFP (n = 4) mice (right).

(J) RNAscope *in situ* hybridization showing colocalization of GFP, Vglut2, and Vgat mRNA in the OVLT of Agtr1a-2A-Cre mice crossed to a GFP reporter line (left; scale bars, 100 μm). Quantification (right; n = 201 cells from 2 mice).

Values are reported as mean ± SEM. *p < 0.05; **p < 0.01; ***p < 0.001; ****p < 0.0001. See also Figure S2.

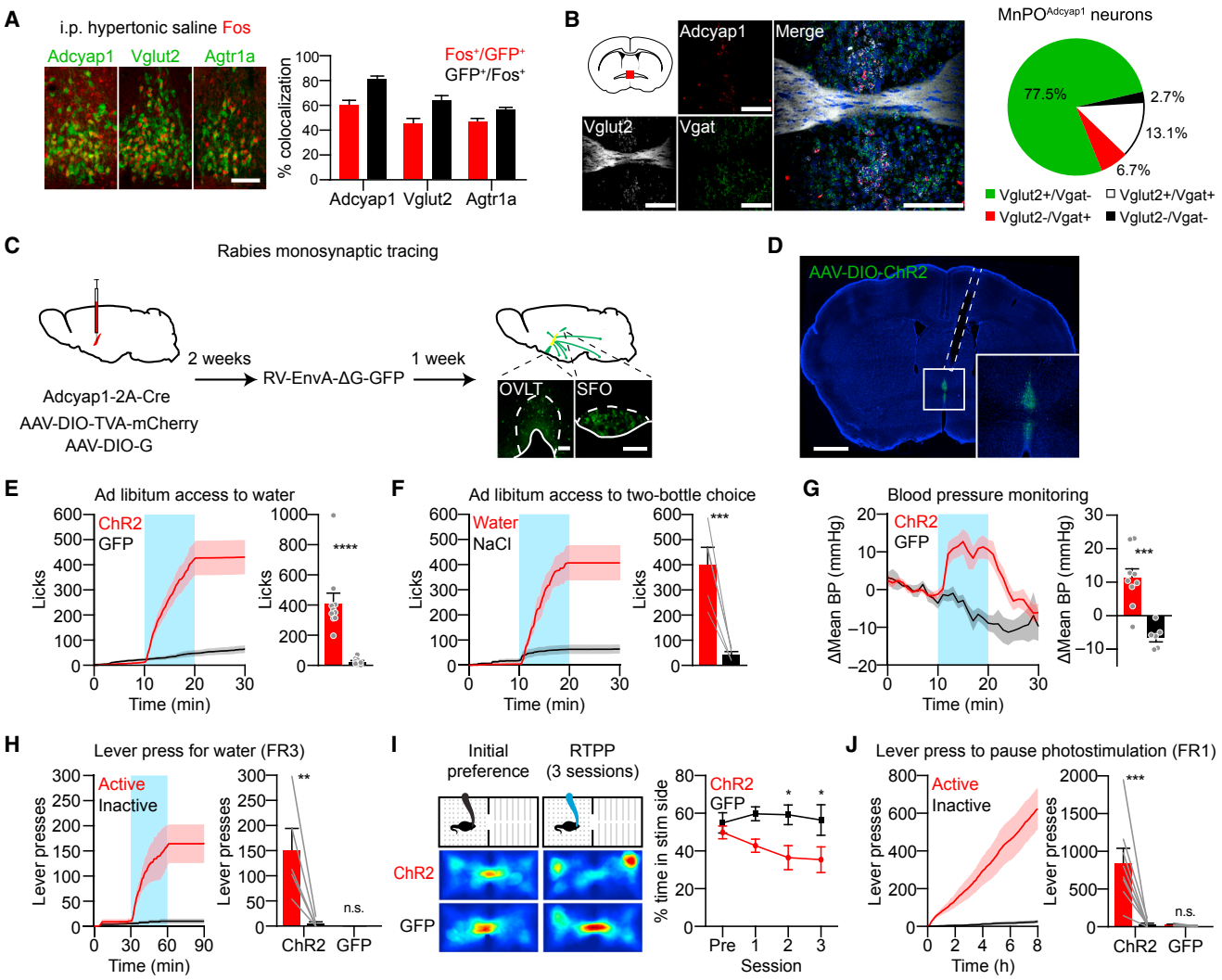

Figure 3. MnPO Thirst Neurons Are Negatively Reinforcing

(A) Colocalization of Fos with Adcyap1 (n = 4), Vglut2 (n = 3), and Agtr1a (n = 3) in the MnPO following salt challenge. Scale bar, 30 μm.

(B) RNAscope *in situ* colocalization of *Adcyap1*, Vglut2, and Vgat (left; scale bars, 200 μm). Quantification (right; 239 cells from 3 mice).

(C) Monosynaptic retrograde rabies tracing from MnPO^{Adcyap1} neurons. Scale bars, 200 μm.

(D) Injection site and fiber placement (dashed line) in MnPO^{Adcyap1} ChR2 mice. Scale bar, 1 mm. (E) Cumulative drinking (left) and total drinking during photostimulation (right) by ChR2 (n = 10) and GFP (n = 9) mice.

(F) Cumulative drinking (left) and total drinking during photostimulation (right) by ChR2 mice (n = 5) during two-bottle choice assay with water and 0.3 M NaCl.

(G) Change in mean arterial blood pressure over time (left) and average photostimulation-induced change (right) in ChR2 (n = 9) and GFP (n = 6) mice.

(H) Cumulative lever pressing for water by ChR2 mice (n = 5) (left) and total lever presses during photostimulation by ChR2 (n = 5) and GFP (n = 3) mice (right).

(I) Real-time, place-preference assay with location heatmaps of individual ChR2 and GFP mice from pre-conditioning and third session of conditioning (left). Percent time spent in photostimulation-paired chamber by ChR2 (n = 6) and GFP (n = 6) mice (right).

(J) Cumulative lever pressing to pause photostimulation by ChR2 mice (n = 8) (left). Lever presses by ChR2 (n = 8) and GFP (n = 4) mice in the negative-reinforcement experiment (right).

Values are reported as mean ± SEM. *p < 0.05, **p < 0.01, ***p < 0.001, ****p < 0.0001. See also Figure S3.

MnPO^{Adcyap1} Neurons Are Activated by Hyperosmolarity and Receive Input from the SFO and OVLT

Signals from the SFO and OVLT are thought to converge on the MnPO (Bourque, 2008; McKinley et al., 2015; Zimmerman et al., 2017). To identify the MnPO neurons that control drinking behavior, we first identified several genes enriched in the MnPO relative to adjacent structures (including *Adcyap1*, *Agtr1a*, and *Slc17a6*) and then measured co-localization between these candidate markers and Fos induced by salt challenge (Figure 3A). This revealed that most Fos$^+$ MnPO neurons express Adcyap1 (81% ± 3%) and, conversely, that most Adcyap1$^+$ neurons express salt challenge-induced Fos (60% ± 4%). A similar, but somewhat lesser, degree of co-localization was observed between Fos and the markers *Agtr1a* and

Slc17a6 (Figure 3A). Consistent with these results, we found that most MnPO^{Adcyap1} neurons express *Slc17a6* (Vglut2), but not *Slc32a1* (Vgat), indicating that these cells are predominantly glutamatergic (Figure 3B). These findings are supported by recent single-cell RNA sequencing data showing that *Adcyap1*, *Agtr1a*, and *Slc17a6* are all enriched in MnPO neurons that express Fos in response to dehydration (Allen et al., 2017).

To demonstrate that MnPO^{Adcyap1} neurons receive input from other structures that drive drinking, we performed cell-type-specific retrograde tracing by targeting the monosynaptic rabies virus to MnPO^{Adcyap1} neurons using an Adcyap1-2A-Cre mouse (Figure 3C). This revealed that MnPO^{Adcyap1} neurons receive strong, monosynaptic input from the SFO and OVLT (Figure 3C) as well as weaker input from several other structures (Figure S3A). Thus, these cells are activated by salt challenge and receive direct input from the SFO and OVLT, strongly suggesting that they are involved in the control of drinking behavior.

Stimulation of MnPO^{Adcyap1} Neurons Drives Drinking and Hypertension

To directly test the function of these cells, we targeted ChR2 to MnPO^{Adcyap1} neurons and positioned an optical fiber above the MnPO (Figure 3D). Photostimulation of MnPO^{Adcyap1} neurons caused rapid drinking behavior that was time-locked to the onset of stimulation (Figure 3E) and specific to water relative to hypertonic NaCl (Figure 3F) and food (Figure S3). Stimulation of MnPO^{Adcyap1} neurons also caused a rapid and reversible increase in blood pressure (Figure 3G; Figure S3). None of these responses were observed in control mice expressing GFP in MnPO^{Adcyap1} neurons (Figures 3E and 3G). We also observed no thermoregulatory response following stimulation of MnPO^{Adcyap1} neurons (Figure S3D), consistent with the dorsocaudal location of MnPO^{Adcyap1} neurons relative to the VMPO^{Adcyap1} neurons previously shown to regulate body temperature (Tan et al., 2016). In addition, stimulation of the largely overlapping MnPO^{Vglut2} neuron population (Figure 3B) recapitulated the behavioral effects of MnPO^{Adcyap1} neuron stimulation (Figures S3H and S3I). Thus, activation of MnPO^{Adcyap1} neurons is sufficient to selectively drive the homeostatic responses to fluid imbalance.

Stimulation of MnPO^{Adcyap1} Neurons Is Negatively Reinforcing

We next investigated the motivational mechanisms by which MnPO^{Adcyap1} neurons drive drinking behavior. We first tested mice in an FR3 task, which revealed that photostimulation of MnPO^{Adcyap1} neurons caused otherwise water-sated mice to vigorously and preferentially press the active lever to receive water (Figure 3H). This demonstrates that stimulation of MnPO^{Adcyap1} neurons drives instrumental responding for water and therefore that these cells promote drinking through a specific change in motivational state.

To characterize the nature of this motivational signal, we measured the valence of MnPO^{Adcyap1} neuron activity using a real-time, place-preference test in which mice were selectively photostimulated when they occupied one chamber of a two-chamber testing apparatus (Figure 3I). At baseline, ChR2 mice showed no preference between the two chambers, but upon testing, they quickly developed a preference for the side without photostimulation (Figure 3I). In contrast, control mice developed no chamber preference despite repeated testing (Figure 3I). This indicates that activation of MnPO^{Adcyap1} neurons is aversive.

To determine whether this aversive signal is sufficient to motivate instrumental responding, we tested whether mice would lever press to block photostimulation of MnPO^{Adcyap1} neurons (Figure 3J). We found that mice expressing ChR2 in MnPO^{Adcyap1} neurons exhibited dramatic lever pressing that was specifically directed toward the active lever (Figure 3J). We observed similar operant responding to shut off stimulation of MnPO^{Vglut2} neurons (Figure S3J), whereas control mice showed little or no responding in any assay. Interestingly, mice engaged in significantly more vigorous and specific lever pressing to block stimulation of MnPO^{Adcyap1} neurons compared to otherwise identical experiments involving upstream OVLT^{Agtr1a} and SFO^{GLUT} neurons (850 ± 190 MnPO^{Adcyap1} versus 169 ± 51 SFO^{GLUT} versus 134 ± 45 OVLT^{Agtr1a}, $^{****}p < 0.0001$). This suggests that these upstream signals may converge on the MnPO to generate an integrated motivational output.

MnPO^{Adcyap1} Neuron Projections Dissociate the Behavioral, Affective, and Cardiovascular Outputs of These Cells

Little is known about how information about fluid balance exits the LT to engage downstream brain regions. SFO^{GLUT} neurons promote thirst primarily through innervation of the other LT regions, the OVLT and MnPO, whereas they promote salt appetite through a projection to the bed nucleus of the stria terminalis (BNST) (Matsuda et al., 2017; Zimmerman et al., 2016). To investigate the downstream targets of thirst neurons in the MnPO, we performed anterograde tracing from MnPO^{Adcyap1} neurons using a Cre-dependent AAV expressing synaptophysin-GCaMP6s (Figure 4A). This revealed innervation of a distributed set of downstream structures, including reciprocal projections to the SFO and OVLT (Figure 4B; Figure S4A). Optogenetic stimulation of the retrograde MnPO^{Adcyap1} → SFO pathway was sufficient to induce drinking and increase blood pressure (Figure S4), suggesting that these reciprocal connections may functionally synchronize LT activity.

In addition to the SFO and OVLT, we found that MnPO^{Adcyap1} neurons project to a number of other structures, including the paraventricular hypothalamus (PVH), supraoptic nuclei (SON), lateral hypothalamus (LH), paraventricular thalamus (PVT), arcuate nucleus (ARC), and dorsomedial hypothalamus (DMH) (Figure 4C; Figure S4A). Anterograde tracing from MnPO^{Vglut2} neurons revealed a similar set of projection targets (Figure S4B). As these structures have been linked to ingestive behavior, valence, and cardiovascular regulation, they represent candidates to mediate the behavioral and autonomic effects of LT stimulation.

To probe the function of these pathways, we targeted ChR2 to MnPO^{Adcyap1} neurons and positioned an optical fiber above the PVH, LH, or PVT to enable photostimulation of MnPO^{Adcyap1} neuron terminals in these regions (Figures 4D, 4H, and 4L). Stimulation of all three sites induced voracious drinking that was time-locked to the onset of stimulation and absent from control mice (Figures 4E, 4I, and 4M). Photostimulation of terminals in the PVH and LH, but not the PVT, also induced a rapid increase

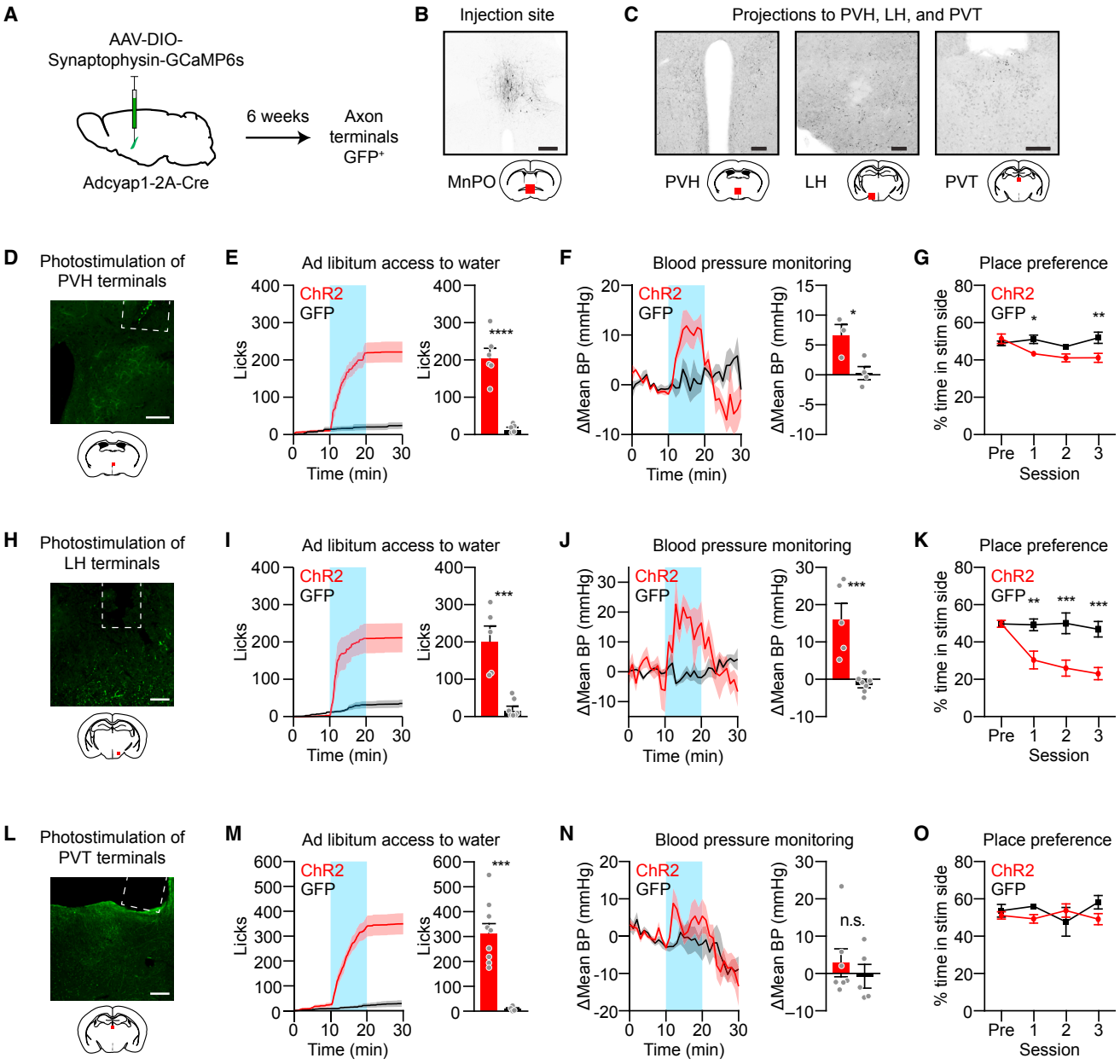

Figure 4. MnPO^{Adcyap1} Neuron Projections Dissociate the Behavioral, Affective, and Cardiovascular Effects of Dehydration

(A) Anterograde tracing strategy.

(B) Example injection site. Scale bar, 200 μm.

(C) MnPO^{Adcyap1} projections to PVH, LH, and PVT. Scale bars, 100 μm.

(D, H, and L) Implant sites (dashed lines) above the PVH (D), LH (H), and PVT (L). Scale bars, 100 μm.

(E, I, and M) Cumulative drinking (left) and total drinking during photostimulation (right) for terminal stimulation in the PVH (E; n = 6 ChR2, n = 5 GFP), LH (I; n = 5 ChR2, n = 7 GFP), and PVT (M; n = 9 ChR2, n = 4 GFP).

(F, J, and N) Change in mean arterial blood pressure over time (left) and average photostimulation-induced change (right) for terminal stimulation in the PVH (F; n = 3 ChR2, n = 5 GFP), LH (J; n = 5 ChR2, n = 7 GFP), and PVT (N; n = 7 ChR2, n = 5 GFP).

(G, K, and O) Percent time spent in photostimulation-paired chamber for terminal stimulation in the PVH (G; n = 4 ChR2, n = 5 GFP), LH (K; n = 5 ChR2, n = 7 GFP), and PVT (O; n = 5 ChR2, n = 4 GFP).

Values are reported as mean ± SEM. *p < 0.05, **p < 0.01, ***p < 0.001, ****p < 0.0001. See also Figure S4.

in blood pressure (Figures 4F, 4J, and 4N; Figure S4D). This indicates that the effects of MnPO^{Adcyap1} neuron activation on drinking and blood pressure can be anatomically dissociated.

We next investigated the motivational properties of these projections. Using a real-time, place-preference test, we found that photostimulation of terminals in the PVH and LH, but not the PVT, was aversive (Figures 4G, 4K, and 4O). Surprisingly, the aversive signal was not strong enough to motivate lever pressing to shut off photostimulation of any of these structures (Figure S4G). This may be, in part, because the valence of MnPO^{Adcyap1} neuron activity is diluted as it is partitioned across multiple anatomic pathways (Figure S4A). Taken together, these data reveal that the behavioral, motivational, and autonomic responses to fluid imbalance, which are unified within the LT, are differentially distributed as they exit the LT via projections of the MnPO.

DISCUSSION

Negative Reinforcement Is a Mechanism that Drives Ingestive Behavior

The nature of the motivational processes that drive eating and drinking has long been debated (Berridge, 2004; Cabanac, 1971; Hull, 1943; Spence, 1956; Toates, 1986). The drive-reduction hypothesis emphasized the fact that hunger and thirst are aversive states and therefore that animals may eat or drink to reduce this unpleasant sensation (Hull, 1943; Spence, 1956). However, this idea was challenged by classic experiments showing that electrical stimulation of the LH, which promotes feeding, is rewarding rather than aversive (Berridge, 2004; Olds and Milner, 1954; Stuber and Wise, 2016). Consistent with this, recent experiments have identified several neural populations that drive food intake and also support self-stimulation and, therefore, may act by positive reinforcement (Chen et al., 2016; Douglass et al., 2017; Jennings et al., 2013). In contrast, although several neural cell types that promote eating or drinking have been shown to exhibit negative valence, none have yet been shown to support operant responding to reduce neural activity, which is the hallmark of negative-reinforcement learning. Thus, direct confirmation that neural circuits motivate ingestive behavior by this mechanism has been lacking.

We have shown here that stimulation of three different cell types distributed throughout the LT, as well as stimulation of projections connecting these neurons, is sufficient to drive drinking and, furthermore, that mice will perform operant tasks for the sole purpose of blocking stimulation of any of these neurons or projections. In addition, while this manuscript was in review, a separate study showed that stimulation of MnPO neurons that express Fos in response to dehydration drives drinking and is negatively reinforcing (Allen et al., 2017). These findings strongly suggest that mice are motivated to find and consume water because they want to reduce the activity of thirst-promoting cells in the LT, consistent with the predictions of the drive-reduction hypothesis (Hull, 1943; Spence, 1956).

The Natural Dynamics of the Thirst Circuit Are Consistent with a Negative-Reinforcement Mechanism

Optogenetic manipulations can reveal the capabilities of a neural circuit, but the meaning of these manipulations can only be understood in the context of the natural dynamics of the circuit during behavior. While the optogenetic data presented here suggest that mice drink water to reduce the activity of their LT neurons, this interpretation requires that LT neurons are actually inhibited during the natural process of drinking.

We recently measured the natural dynamics of SFO^{GLUT} neurons during drinking behavior and discovered that this is indeed the case (Zimmerman et al., 2016). SFO^{GLUT} neurons are highly active when mice are thirsty and then become progressively inhibited each time a mouse takes a lick of water, which continues until the neurons return to baseline activity and drinking terminates (Zimmerman et al., 2016). This activity pattern is precisely what would be predicted for a neural population that motivates behavior by negative reinforcement (Berridge, 2004). Moreover, it was recently shown that vasopressin neurons in the PVH and SON, which are downstream of SFO^{GLUT} neurons, display very similar dynamics during drinking (Mandelblat-Cerf et al., 2017), as do MnPO neurons that are activated by dehydration (Allen et al., 2017). It therefore appears likely that the LT as a whole is regulated in this manner, consistent with the data presented here showing that each node shares common motivational properties.

While it may seem intuitive that a neuron driving ingestive behavior would be progressively inhibited during satiation, thereby gradually reducing an aversive drive, this result is not guaranteed. Indeed, it was long assumed that AgRP neurons that control hunger would display these dynamics during food intake, but they do not. AgRP neurons are instead inhibited the moment that a mouse detects food, and critically, they are not further inhibited during the course of eating (Betley et al., 2015; Chen et al., 2015; Mandelblat-Cerf et al., 2015). Consistent with this result, the activity of AgRP neurons is not negatively reinforcing (Betley et al., 2015; Chen et al., 2016) but instead supports self-stimulation (Chen et al., 2016). Thus, the data presented here reveal that interoceptive neurons that control hunger and thirst utilize fundamentally different mechanisms to motivate behavior.

The Functional Outputs of the LT Are Distributed along Multiple Anatomic Pathways

For more than 40 years, research into the neurobiology of thirst has focused on the LT (Bourque, 2008; Leib et al., 2016; McKinley and Johnson, 2004; Noda and Sakuta, 2013; Zimmerman et al., 2017). These studies have established a critical role for the LT in a broad range of homeostatic responses, including not only thirst, but also salt appetite, blood pressure control, and vasopressin release. What has remained unclear, however, is how information from the LT exits this circuitry to communicate with downstream brain regions that directly control the motor, cardiovascular, and motivational aspects of fluid homeostasis.

In this study, we have identified neurons in all three LT structures that are sufficient to drive the behavioral and autonomic responses to fluid imbalance. By obtaining genetic access to these cells, we have further been able to visualize their projections and test their function. Signals from the SFO and OVLT are thought to converge on the MnPO, and consistent with this, we have shown that stimulation of MnPO neurons has stronger motivational effects than stimulation of analogous cells in the SFO or OVLT.

This suggests that MnPO activation is the mechanism by which these upstream structures generate valence, but it does not rule out more complex mechanisms involving other brain regions. Addressing this question will require further studies that map the functional connectivity between genetically defined cell types in these three structures and their downstream targets.

We have shown that MnPO^{Adcyap1} neurons project broadly to brain regions outside the LT, suggesting that these cells may function as the output node of the LT thirst circuit. Stimulation of MnPO^{Adcyap1} neuron projections innervating three structures (PVH, LH, and PVT) revealed that all three pathways are sufficient to drive drinking behavior, similar to recent observations for MnPO neurons that are activated by dehydration (Allen et al., 2017). We found that these projections differ in their ability to recapitulate the motivational/affective and cardiovascular responses to fluid imbalance. These results reveal that some functional outputs of the LT are anatomically segregated, whereas others are redundantly distributed. An important task for the future will be to identify and characterize the thirst-promoting cells in each of these downstream targets, in order to understand how the LT transforms chemical information about fluid balance into a coordinated, homeostatic response.

STAR★METHODS

Detailed methods are provided in the online version of this paper and include the following:

- KEY RESOURCES TABLE
- CONTACT FOR REAGENT AND RESOURCE SHARING
- EXPERIMENTAL MODEL AND SUBJECT DETAILS
- METHOD DETAILS
  - Generation of the Agtr1a-2a-Cre Mouse Line
  - Stereotaxic Surgery
  - GFP-Reporter Labeling and Cell Counts
  - Virus Validation by Acute Slice Electrophysiology
  - Photostimulation *In Vivo*
  - Blood Pressure Measurements
  - Real-Time Place Preference
  - Immunohistochemistry
  - *In Situ* Hybridization
- QUANTIFICATION AND STATISTICAL ANALYSIS

SUPPLEMENTAL INFORMATION

Supplemental Information includes four figures and can be found with this article online at https://doi.org/10.1016/j.neuron.2017.11.041.

ACKNOWLEDGMENTS

D.E.L. acknowledges support from the ARCS Foundation Scholarship, UCSF Discovery Fellowship, and NIH NRSA Predoctoral Fellowship (F31-HL131463). C.A.Z. acknowledges support from the Genentech Foundation Predoctoral Fellowship, UCSF Discovery Fellowship, NSF Graduate Research Fellowship (1144247), and NIH NRSA Predoctoral Fellowship (F31-HL137383). Z.A.K. is a New York Stem Cell Foundation-Robertson Investigator. Z.A.K. acknowledges support from the New York Stem Cell Foundation, the American Diabetes Association Pathway Program, the Rita Allen Foundation, the McKnight Foundation, the Alfred P. Sloan Foundation, the Brain and Behavior Research Foundation, the Esther A. & Joseph Klingenstein Foundation, the Program for Breakthrough Biological Research, and the UCSF DERC (P30-DK06372) and NORC (P30-DK098722). This work was supported by an NIH New Innovator Award (DP2-DK109533), R01-NS094781, and R01-DK106399.

AUTHOR CONTRIBUTIONS

D.E.L., C.A.Z., and Z.A.K. conceived the project and designed the experiments. D.E.L. and C.A.Z. performed stereotaxic surgeries and conducted behavioral experiments. A.P. and E.L.H. also performed stereotaxic surgeries, and A.P. conducted some behavioral experiments. J.S.A. performed in situs, Y.-C.L. performed electrophysiology experiments, and C.L.T. performed thermoregulation experiments. C.A.Z. generated the Agtr1a-2A-Cre mouse with initial help from Y.C. D.E.L., C.A.Z., and Z.A.K. analyzed the data and prepared the manuscript with input from all authors.

DECLARATION OF INTERESTS

The authors declare no competing interests.

Received: September 8, 2017
Revised: November 9, 2017
Accepted: November 30, 2017
Published: December 20, 2017

SUPPORTING CITATIONS

The following reference appears in the Supplemental Information: Romanov et al. (2017).

REFERENCES

Abbott, S.B.G., Machado, N.L.S., Geerling, J.C., and Saper, C.B. (2016). Reciprocal control of drinking behavior by median preoptic neurons in mice. J. Neurosci. *36*, 8228–8237.

Allen, W.E., DeNardo, L.A., Chen, M.Z., Liu, C.D., Loh, K.M., Fenno, L.E., Ramakrishnan, C., Deisseroth, K., and Luo, L. (2017). Thirst-associated preoptic neurons encode an aversive motivational drive. Science *357*, 1149–1155.

Berridge, K.C. (2004). Motivation concepts in behavioral neuroscience. Physiol. Behav. *81*, 179–209.

Betley, J.N., Xu, S., Cao, Z.F.H., Gong, R., Magnus, C.J., Yu, Y., and Sternson, S.M. (2015). Neurons for hunger and thirst transmit a negative-valence teaching signal. Nature *521*, 180–185.

Bourque, C.W. (2008). Central mechanisms of osmosensation and systemic osmoregulation. Nat. Rev. Neurosci. *9*, 519–531.

Buggy, J., and Jonhson, A.K. (1977). Preoptic-hypothalamic periventricular lesions: thirst deficits and hypernatremia. Am. J. Physiol. *233*, R44–R52.

Cabanac, M. (1971). Physiological role of pleasure. Science *173*, 1103–1107.

Chen, Y., Lin, Y.-C., Kuo, T.-W., and Knight, Z.A. (2015). Sensory detection of food rapidly modulates arcuate feeding circuits. Cell *160*, 829–841.

Chen, Y., Lin, Y.-C., Zimmerman, C.A., Essner, R.A., and Knight, Z.A. (2016). Hunger neurons drive feeding through a sustained, positive reinforcement signal. eLife *5*, e18640.

Crews, E.C., and Rowland, N.E. (2005). Role of angiotensin in body fluid homeostasis of mice: effect of losartan on water and NaCl intakes. Am. J. Physiol. Regul. Integr. Comp. Physiol. *288*, R638–R644.

Douglass, A.M., Kucukdereli, H., Ponserre, M., Markovic, M., Gründemann, J., Strobel, C., Alcala Morales, P.L., Conzelmann, K.-K., Lüthi, A., and Klein, R. (2017). Central amygdala circuits modulate food consumption through a positive-valence mechanism. Nat. Neurosci. *20*, 1384–1394.

Gonzalez, A.D., Wang, G., Waters, E.M., Gonzales, K.L., Speth, R.C., Van Kempen, T.A., Marques-Lopes, J., Young, C.N., Butler, S.D., Davisson, R.L., et al. (2012). Distribution of angiotensin type 1a receptor-containing cells in the brains of bacterial artificial chromosome transgenic mice. Neuroscience *226*, 489–509.

Hull, C.L. (1943). Principles of Behavior: An Introduction to Behavior Theory (Appleton-Century-Crofts).

Jennings, J.H., Rizzi, G., Stamatakis, A.M., Ung, R.L., and Stuber, G.D. (2013). The inhibitory circuit architecture of the lateral hypothalamus orchestrates feeding. Science *341*, 1517–1521.

Leib, D.E., Zimmerman, C.A., and Knight, Z.A. (2016). Thirst. Curr. Biol. *26*, R1260–R1265.

Lenkei, Z., Palkovits, M., Corvol, P., and Llorens-Cortès, C. (1997). Expression of angiotensin type-1 (AT1) and type-2 (AT2) receptor mRNAs in the adult rat brain: a functional neuroanatomical review. Front. Neuroendocrinol. *18*, 383–439.

Mandelblat-Cerf, Y., Ramesh, R.N., Burgess, C.R., Patella, P., Yang, Z., Lowell, B.B., and Andermann, M.L. (2015). Arcuate hypothalamic AgRP and putative POMC neurons show opposite changes in spiking across multiple timescales. eLife *4*, e07122.

Mandelblat-Cerf, Y., Kim, A., Burgess, C.R., Subramanian, S., Tannous, B.A., Lowell, B.B., and Andermann, M.L. (2017). Bidirectional anticipation of future osmotic challenges by vasopressin neurons. Neuron *93*, 57–65.

Mangiapane, M.L., and Simpson, J.B. (1980). Subfornical organ: forebrain site of pressor and dipsogenic action of angiotensin II. Am. J. Physiol. *239*, R382–R389.

Matsuda, T., Hiyama, T.Y., Niimura, F., Matsusaka, T., Fukamizu, A., Kobayashi, K., Kobayashi, K., and Noda, M. (2017). Distinct neural mechanisms for the control of thirst and salt appetite in the subfornical organ. Nat. Neurosci. *20*, 230–241.

McKinley, M.J., and Johnson, A.K. (2004). The physiological regulation of thirst and fluid intake. News Physiol. Sci. *19*, 1–6.

McKinley, M.J., McAllen, R.M., Davern, P., Giles, M.E., Penschow, J., Sunn, N., Uschakov, A., and Oldfield, B.J. (2003). The sensory circumventricular organs of the mammalian brain. Adv. Anat. Embryol. Cell Biol. *172*, III–XII, 1–122, back cover.

McKinley, M.J., Yao, S.T., Uschakov, A., McAllen, R.M., Rundgren, M., and Martelli, D. (2015). The median preoptic nucleus: front and centre for the regulation of body fluid, sodium, temperature, sleep and cardiovascular homeostasis. Acta Physiol. (Oxf.) *214*, 8–32.

Nation, H.L., Nicoleau, M., Kinsman, B.J., Browning, K.N., and Stocker, S.D. (2016). DREADD-induced activation of subfornical organ neurons stimulates thirst and salt appetite. J. Neurophysiol. *115*, 3123–3129.

Noda, M., and Sakuta, H. (2013). Central regulation of body-fluid homeostasis. Trends Neurosci. *36*, 661–673.

Oka, Y., Ye, M., and Zuker, C.S. (2015). Thirst driving and suppressing signals encoded by distinct neural populations in the brain. Nature *520*, 349–352.

Olds, J., and Milner, P. (1954). Positive reinforcement produced by electrical stimulation of septal area and other regions of rat brain. J. Comp. Physiol. Psychol. *47*, 419–427.

Romanov, R.A., Zeisel, A., Bakker, J., Girach, F., Hellysaz, A., Tomer, R., Alpár, A., Mulder, J., Clotman, F., Keimpema, E., et al. (2017). Molecular interrogation of hypothalamic organization reveals distinct dopamine neuronal subtypes. Nat. Neurosci. *20*, 176–188.

Slotnick, B. (2009). A simple 2-transistor touch or lick detector circuit. J. Exp. Anal. Behav. *91*, 253–255.

Spence, K.W. (1956). Behavior Theory & Conditioning (Yale University Press).

Stuber, G.D., and Wise, R.A. (2016). Lateral hypothalamic circuits for feeding and reward. Nat. Neurosci. *19*, 198–205.

Tan, C.L., Cooke, E.K., Leib, D.E., Lin, Y.-C., Daly, G.E., Zimmerman, C.A., and Knight, Z.A. (2016). Warm-sensitive neurons that control body temperature. Cell *167*, 47–59.e15.

Teitelbaum, P. (1966). The use of operant methods in the assessment and control of motivational states. In Operant Behavior: Areas of Research & Application, W.K. Honig, ed. (Appleton-Century-Crofts), pp. 565–608.

Toates, F.M. (1986). Motivational Systems (Cambridge University Press).

Zimmerman, C.A., Lin, Y.-C., Leib, D.E., Guo, L., Huey, E.L., Daly, G.E., Chen, Y., and Knight, Z.A. (2016). Thirst neurons anticipate the homeostatic consequences of eating and drinking. Nature *537*, 680–684.

Zimmerman, C.A., Leib, D.E., and Knight, Z.A. (2017). Neural circuits underlying thirst and fluid homeostasis. Nat. Rev. Neurosci. *18*, 459–469.

STAR★METHODS

KEY RESOURCES TABLE

REAGENT or RESOURCE	SOURCE	IDENTIFIER
Antibodies		
Rabbit polyclonal anti-Fos	Santa Cruz Biotechnology	Cat#sc-52; RRID: AB_2106783
Chicken polyclonal anti-GFP	Aves Labs	Cat#GFP-1020; RRID: AB_10000240
Rat monoclonal anti-RFP	ChromoTek	Cat#5f8-100; RRID: AB_2336064
Bacterial and Virus Strains		
AAV5-EF1a-DIO-hChR2(H134R)-EYFP	UNC Vector Core	N/A
AAV2-EF1a-Flex-EGFP-L10a	Tan et al., 2016; Zimmerman et al., 2016; produced by UNC Vector Core	N/A
AAV5-Camk2-hChR2(E123T/T159C)-2A-mCherry	UNC Vector Core	N/A
AAV5-Ef1a-DIO-hChR2(E123T/T159C)-2A-mCherry	UNC Vector Core	N/A
AAV5-Camk2-GFP	UNC Vector Core	N/A
AAVDJ-Ef1a-DIO-synaptophysin-GCaMP6s	Zimmerman et al., 2016; produced by Stanford Vector Core	N/A
AAV1-CAG-DIO-TVA-mCherry	Zimmerman et al., 2016; obtained from laboratory of N. Shah	N/A
AAV1-CAG-DIO-G	Zimmerman et al., 2016; obtained from laboratory of N. Shah	N/A
RV-EnvA-ΔG-GFP	Salk Institute	N/A
Critical Commercial Assays		
RNAscope Fluorescent Multiplex Kit	Advanced Cell Diagnostics	Probes: Slc32a1, Cat#319191/319191-C3; Slc17a6, Cat#319171-C2; eGFP, Cat# 400281-C3; Adcyap1, Cat#405911
Experimental Models: Organisms/Strains		
Mouse: wild-type (C57BL/6J)	The Jackson Laboratory	Strain#000664; RRID: IMSR_JAX:000664
Mouse: Agtr1a-2A-Cre knockin	This paper	N/A
Mouse: Adcyap1-2A-Cre knockin (B6.Cg-*Adcyap1*$^{tm1.1(cre)Hze}$/ZakJ)	Tan et al., 2016; originally obtained from Allen Brain Institute	The Jackson Laboratory Strain#030155; RRID: IMSR_JAX:030155
Mouse: Slc17a6-IRES-Cre knockin (Slc17a6$^{tm2(cre)Lowl}$/J)	The Jackson Laboratory	Strain#016963; RRID: IMSR_JAX:016963
Mouse: Nos1-IRES-Cre knockin (Nos1$^{tm1(Cre)Mgmj}$/J)	The Jackson Laboratory	Strain#017526; RRID: IMSR_JAX:017526
Mouse: Agtr1a-GFP BAC transgene (Tg(Agtr1aEGFP)NZ44Gsat)	MMRRC	Strain#033059; RRID: MMRRC_033059-UCD
Mouse: Ai32 (B6.129S-Gt(ROSA) 26Sor$^{tm32(CAG-COP4*H134R/EYFP)Hze}$/J)	The Jackson Laboratory	Strain#012569; RRID: IMSR_JAX:012569
Mouse: Ai40D (B6.Cg-Gt(ROSA) 26Sor$^{tm40.1(CAG-aop3/EGFP)Hze}$/J)	The Jackson Laboratory	Strain#021188; RRID: IMSR_JAX:021188
Mouse: Rosa26$^{fs-GFPL10}$ (B6.129S4-Gt(ROSA) 26Sor$^{tm1(CAG-EGFP/Rpl10a,-birA)Wtp}$/J)	The Jackson Laboratory	Strain#022367; RRID: IMSR_JAX:022367
Mouse: Gad2-2A-NLS-mCherry knockin (B6;129S-*Gad2*$^{tm1.1Ksvo}$/J)	The Jackson Laboratory	Strain#023140; RRID: IMSR_JAX:023140
Oligonucleotides		
Agtr1a-2A-Cre long range PCR primer, forward (CGAGCCTGTGAGGTTAAAGAT)	Integrated DNA Technologies	N/A
Agtr1a-2A-Cre long range PCR primer, reverse (GCGCGCCTGAAGATATAGAA)	Integrated DNA Technologies	N/A

(*Continued on next page*)

Continued

REAGENT or RESOURCE	SOURCE	IDENTIFIER
Software and Algorithms		
MATLAB R2017A	MathWorks	N/A
Prism 7	GraphPad	N/A
Fiji	ImageJ	N/A

CONTACT FOR REAGENT AND RESOURCE SHARING

Further information and requests for reagents may be directed to and will be fulfilled by the corresponding author, Zachary Knight (zachary.knight@ucsf.edu).

EXPERIMENTAL MODEL AND SUBJECT DETAILS

All animals were maintained on a 12-h light/dark cycle and given *ad libitum* access to chow (PicoLab Rodent Diet 5053) and water. All transgenic mice used in these studies were on the C57BL/6J background, except Agtr1a-2A-Cre mice that were maintained on a mixed FVB/C57BL/6J background. Unless otherwise stated, all studies employed a mixture of male and female mice and no differences between sexes were observed. All procedures were conducted during the light cycle unless otherwise noted. All experimental protocols were approved by the University of California, San Francisco IACUC following the National Institutes of Health guidelines for the Care and Use of Laboratory Animals.

METHOD DETAILS

Wild-type mice (C57BL/6J, strain 000664), Slc17a6-IRES-Cre mice (Slc17a6$^{tm2(cre)Lowl}$/J, strain 016963), Nos1-IRES-Cre mice (Nos1$^{tm1(Cre)Mgmj}$/J, strain 017526), Gad2-2A-NLS-mCherry mice (B6;129S-*Gad2*$^{tm1.1Ksvo}$/J, strain 023140), Rosa26-LSL-hChR2 (H134R)-eYFP mice (Ai32; B6.129S-Gt(ROSA)26Sor$^{tm32(CAG-COP4*H134R/EYFP)Hze}$/J, strain 012569), Rosa26-LSL-LSL-ArchT-eGFP mice (Ai40D; B6.Cg-Gt(ROSA)26Sor$^{tm40.1(CAG-aop3/EGFP)Hze}$/J, strain 021188), and Rosa26-LSL-GFPL10 mice (B6.129S4-Gt(ROSA)26Sor$^{tm1(CAG-EGFP/Rpl10a,-birA)Wtp}$/J, strain 022367) were obtained from the Jackson Laboratory. Adcyap1-2A-Cre mice were obtained from the Allen Institute. Agtr1a-GFP mice (Tg(Agtr1aEGFP)NZ44Gsat, strain 033059) were obtained from MMRRC. Recombinant AAVs expressing hChR2(H134R) (AAV5-Ef1a-DIO-hChR2(H134R)-eYFP), hChR2(E123T/T159C) (AAV5-Camk2-hChR2(E123T/T159C)-2A-mCherry, AAV5-Ef1a-DIO-hChR2(E123T/T159C)-2A-mCherry), and GFP (AAV5-Camk2-GFP) were obtained from the UNC Vector Core. Recombinant EnvA-pseudotyped G-deficient rabies virus expressing GFP (RV-EnvA-ΔG-GFP) was obtained from the Salk Institute. Plasmids encoding synaptophysin-GCaMP6s and GFP-RPL10a fusion proteins were generated in-house, and recombinant AAVs containing these plasmids (AAV5-EF1a-DIO-synaptophysin-GCaMP6s; AAV2-EF1a-FLEX-GFP-RPL10a) were commercially produced by the UNC Vector Core (Tan et al., 2016; Zimmerman et al., 2016). Rabies helper viruses (AAV1-CAG-DIO-TVA-mCherry; AAV1-CAG-DIO-G) were obtained from the laboratory of Nirao Shah.

Generation of the Agtr1a-2a-Cre Mouse Line

The bicistronic Agtr1a-2A-Cre allele was generated by homologous recombination at the endogenous *Agtr1a* locus, aided by targeted CRISPR endonuclease activity. Briefly, homology regions were captured into a plasmid from a BAC containing the *Agtr1a* locus by recombineering. The T2A-Cre sequence was inserted immediately upstream of the endogenous stop codon. The final targeting vector contained ~2 kb (5′) and ~7 kb (3′) homology arms and was verified by restriction digest and sequencing. To generate site-specific double stranded breaks using CRISPR, an sgRNA sequence (TTGTTCTGAGGTGGAGTGAC) was selected such that the guide sequence would be separated from the PAM site in the genomic DNA by the 2A-Cre insertion. This ensured that the targeting vector and recombined *Agtr1a-2a-Cre* allele were protected from Cas9 nuclease activity. Super-ovulated female FVB/N mice were mated to FVB/N stud males, and fertilized zygotes were collected from oviducts. Cas9 protein (100 ng/μL), sgRNA (250 ng/μL) and targeting vector DNA (100 ng/μL) were mixed and injected into the pronucleus of fertilized zygotes. 125 injected zygotes were implanted into oviducts of pseudopregnant CD1 female mice. 18 out of 35 pups genotyped were positive for the knock-in allele, and 16 of these also contained the targeting vector inserted randomly as a transgene. Two independent knock-in lines were crossed to reporter mice, and reporter expression patterns from these lines were identical. All Agtr1a-2A-Cre mice used here were maintained on mixed FVB/C57BL/6J background. Founder pups and offspring were genotyped for the presence of the knock-in allele by qPCR. Presence of the knock-in allele was also verified by long range PCR (expected amplicon size 2496 bp) using a forward PCR primer upstream of the 5′ homology arm (CGAGCCTGTGAGGTTAAAGAT) and a reverse PCR primer inside the Cre sequence (GCGCGCCTGAAGATATAGAA).

Stereotaxic Surgery

Surgeries were conducted on a stereotaxic frame (Kopf). Mice were anesthetized with isoflurane and received bupivacaine, carprofen, and buprenorphine during surgery in accordance with UCSF IACUC guidelines. Injections were performed with pulled glass pipets and 10-μl Hamilton syringes controlled by a micropump (Kopf). Homemade fiberoptic implants were secured to the skull with Vetbond (SCB, sc-361931) and dental cement (A-M Systems 526000). Following surgery, incisions were closed using Vetbond.

All SFO virus injections were in wild-type mice (unless otherwise noted) using the following coordinates: 0 mm M/L, –0.50 mm A/P, –2.75 mm below the surface of the skull. Implants above the SFO were placed using the same coordinates but –2.45 mm below the surface of the skull. Implants above the MnPO were placed at the following coordinates: 0 mm M/L, +0.45 mm A/P, –3.70 mm below the surface of the skull. Wild-type mice were injected with 100–200 nL of AAV5-Camk2-hChR2(E123T/T159C)-2A-mCherry or AAV5-Camk2-GFP. For fasting-refeeding experiments, Nos1-IRES-Cre mice were injected with 100–200 nL of AAV5-Ef1a-DIO-hChR2(E123T/T159C)-2A-mCherry.

All OVLT virus injections were in Agtr1a-2A-Cre mice using the following coordinates: 0 mm M/L, +0.40 mm A/P, and –4.75 mm below the surface of the skull. Implants above the OVLT were placed using the same coordinates but –4.55 mm below the surface of the skull. Mice intended for optogenetics experiments were injected with 100 nL of AAV5-Ef1a-DIO-hChR2(H134R)-eYFP (n = 6 mice) or crossed to the Rosa26-LSL-hChR2(H134R)-eYFP reporter line (n = 3 mice). Control mice were crossed to the Rosa26-LSL-GFP-RPL10 reporter line.

All MnPO virus injections were in Adcyap1-2a-Cre mice (unless otherwise noted), angled at 15°, and used the following coordinates: +1.0 mm M/L, +0.45 mm A/P, –4.3 mm below the surface of the skull. Implants above the MnPO were placed using the same angle and coordinates but –3.7 mm below the surface of the skull. Implants for MnPO projection stimulation were placed at the following coordinates: PVH (no angle, −0.3 mm M/L, −0.6 mm A/P, −4.75 mm below the surface of the skull); LH (no angle, −1.0 mm M/L, −1.4 mm A/P, −5.0 mm below the surface of the skull); PVT (15°, +0.8, −0.9 mm A/P, −3.2 mm below the surface of the skull); SFO (15°, +0.8 mm M/L, −0.55 mm A/P, −2.6 mm below the surface of the skull). For Fos/GFP colocalization, 1500 nL of AAV2-EF1α-FLEX-GFP-RPL10a was injected into Adcyap1-2A-Cre or Vglut2-IRES-Cre mice. Mice intended for optogenetics experiments were injected with 100 nL of AAV5-Ef1a-DIO-hChR2(H134R)-eYFP or AAV2-EF1α-FLEX-GFP-RPL10a. For rabies tracing, 75 nL of a 1:1 mix of AAV1-CAG-DIO-TVA-mCherry and AAV1-CAG-DIO-G was injected. After two weeks, 200 nL of recombinant EnvA-pseudotyped G-deficient rabies virus expressing GFP was injected. After one additional week, mice were euthanized and processed for histology. For anterograde tracing, 50 nL of AAV5-EF1α-DIO-synaptophysin-GCaMP6s was injected.

GFP-Reporter Labeling and Cell Counts

To quantify Fos/GFP overlap, 20X Z stack images from 40-μm coronal slices (bregma +0.1 to +0.2 mm) were taken, and the numbers of Fos/GFP double positive or singly positive cells were counted in FIJI.

Virus Validation by Acute Slice Electrophysiology

Acute hypothalamic slices were prepared from Adcyap1-2A-Cre mice expressing AAV5-Ef1a-DIO-hChR2(H134R)-eYFP as previously described (Zimmerman et al., 2016). Briefly, spike fidelity was measured in current clamp with LED light stimulation at 5, 10, 15, and 20 Hz.

Photostimulation *In Vivo*

All experiments were performed in behavioral chambers (Coulbourn Instruments, Habitest Modular System), and water consumption was monitored with contact lickometers (Slotnick, 2009). Mice were acclimated to the behavioral chamber for at least 15 min before the beginning of each testing session. For SFO and OVLT optogenetics experiments, mice were photostimulated with 10-ms pulses at 10 Hz and 10–15 mW laser power, measured from the tip using a DPSS 473-nm laser (Shanghai Laser and Optics Century), except for negative-reinforcement experiments (5 Hz and 10–15 mW laser power) and fasting-refeeding experiments (20 Hz and 10–15 mW laser power). For MnPO soma, $MnPO^{Adcyap1} \rightarrow PVT$, and $MnPO^{Adcyap1} \rightarrow SFO$ optogenetics experiments, mice were photostimulated with 10-ms pulses at 5 Hz and 5–10 mW laser power. For $MnPO^{Adcyap1} \rightarrow PVH$ optogenetics experiments, mice were stimulated at 10 Hz and 10 mW. For $MnPO^{Adcyap1} \rightarrow LH$ optogenetics experiments, mice were stimulated at 20 Hz and 20 mW. The increases in frequency in PVH/LH and laser power in LH photostimulation were the minimum to produce reliable drinking in these mice. To test whether acute photostimulation could induce drinking, mice were provided with constant access to water and monitored for 10 min (pre-stim), then photostimulated for 10 min, and then monitored for another 10 min (post-stim). For NaCl drinking experiments, the same model was used except that mice were provided with access to various NaCl solutions. For negative-reinforcement experiments, mice were photostimulated constantly during the dark cycle. Pressing the active lever turned off the laser for 10 s. For lever pressing for water reward, mice were first trained to receive 5 μL of water for one active lever press (FR1) for at least three nights and then for 3 active lever presses (FR3) for three nights. Then, during the light cycle, lever presses were measured during 30-min pre-stim, stim, and post-stim periods. For SFO^{GLUT} fasting-refeeding experiments, mice were food deprived for 24 hours, then given access to food and water. For *ad libitum* feeding experiments, mice were given access to food but not water, and their food intake was measured during 30-minute pre-stim, stim, and post-stim periods. For $MnPO^{Adcyap1}$ fasting-refeeding experiments, mice were food deprived for 24 hours then given access to food but no water for 30 minutes.

Blood Pressure Measurements

For blood pressure measurements, mice were sedated with medetomidine (50 μg/kg, ApexBio). The sedated mice were then restrained, placed on a warming platform, and their blood pressure measured using the CODA-HT4 Noninvasive Blood Pressure System (Kent Scientific). After a 10-min habituation period, blood pressure was measured once per minute during 10 min pre-stim, stim, and post-stim periods. Data were analyzed using an in-house MATLAB script that subtracted baseline blood pressure for each mouse and compared the change in blood pressure from the pre-stim to stim periods (averaged during the 4^{th} to 10^{th} minute of each period).

Real-Time Place Preference

A custom 2-chamber apparatus (30 cm x 15 cm) was used. The two sides differed in floor texture and wall markings, and the mice were free to move between both sides throughout all experiments. First, baseline preference was recorded for 15 min. During 15 min sessions on the next 3 days, a custom MATLAB script was used to track the mice and pair one side of the chamber with photostimulation. Using a custom MATLAB script, preferences were calculated as percent time spent in the chamber paired with photostimulation.

Immunohistochemistry

Mice were transcardially perfused with PBS followed by formalin. Brains were postfixed overnight in formalin at 4°C and washed with PBS. Free floating sections (40 μm) were prepared with a cryostat, blocked (3% BSA, 2% NGS and 0.1% Triton-X in PBS for two hours), and then incubated with primary antibody overnight at 4°C. Sample were washed three times with wash buffer (1xPBS + 0.1% Triton-X), incubated with secondary antibody for one hour at room temperature, washed again and then mounted and imaged by confocal microscopy. Primary antibodies used were: anti-GFP (Abcam, ab13970, 1:1000), anti-FOS (SCB, sc-52 and sc-52-G), and anti-RFP (Chromotek 5F8, 1:1000).

In Situ Hybridization

In situ hybridization was performed using RNAscope Fluorescent Multiplex Kit (Advanced Cell Diagnostics). Mouse brain tissue was freshly frozen in Tissue-Tek O.C.T Compound, then sectioned into 20 μm sections by cryostat and mounted on Superfrost Plus slides. The sections were fixed in 4% paraformaldehyde (15 min at 4°C), then dehydrated in a series of ethanol washes following the manufacturer's instructions. The sections were treated with Protease IV in a HybEZ Humidity Control Tray (30 min at RT) and then incubated with target probes in a HybEZ Oven (2 h at 40°C). For the MnPO, tissues were probed for *Adcyap1* in C1, *Slc17a6* in C2, and *Slc32a1* in C3. For the OVLT, tissues were probed for *Slc32a1* in C1, *Slc17a6* in C2, and e*GFP* in C3. The sections were treated with Hybridize Amp 1-4 then stained with DAPI Fluoromount-G. The sections were then imaged with a confocal microscope and co-localization manually counted from 20x z stacks.

QUANTIFICATION AND STATISTICAL ANALYSIS

Statistical parameters including sample sizes (n = number of animal subjects per group), the definition of center, and dispersion and precision measures are reported in the Figures and the Figure Legends. Unless otherwise indicated, values are reported as mean ± SEM (error bars or shaded area). P values for pairwise comparisons were performed using a two-tailed Student's t test. P values for all other comparisons were performed using 1-way or 2-way ANOVA followed by post hoc pairwise comparisons using Holm-Šídák multiple comparisons test. All optogenetic trials involved age-matched littermates as controls where possible. Mice were randomly assigned before surgery to either ChR2 or control groups. Data were judged to be statistically significant when $p < 0.05$. In figures, asterisks denote statistical significance *$p < 0.05$, **$p < 0.01$, ***$p < 0.001$, ****$p < 0.0001$. All statistical analysis was performed using GraphPad PRISM 7 software.